Reversible operation of microtubular solid oxide cells using $La_{0.6}Sr_{0.4}Co_{0.2}Fe_{0.8}O_{3-\delta}$-$Ce_{0.9}Gd_{0.1}O_{2-\delta}$ oxygen electrodes

López-Robledo, M.J.[1,2*], Laguna-Bercero, M.A.[1*], Larrea, A.[1] Orera, V.M.[1]

1 Instituto de Ciencia de Materiales de Aragón, CSIC-Universidad de Zaragoza, Zaragoza, Spain.

2 Centro Universitario de la Defensa, General Military Academy, Spain.

*** Corresponding authors:** Dr. M.J. López-Robledo, robledo@unizar.es; Dr. M.A. Laguna-Bercero, malaguna@unizar.es;

Abstract

Yttria stabilized zirconia (YSZ) based microtubular solid oxide fuel cells (mT-SOFCs) using $La_{0.6}Sr_{0.4}Co_{0.2}Fe_{0.8}O_{3-\delta}$ (LSCF) and $Ce_{0.9}Gd_{0.1}O_{2-\delta}$ (GDC) as the oxygen electrode, along with a porous GDC electrolyte-electrode barrier layer, were fabricated and characterized in both fuel cell (SOFC) and electrolysis (SOEC) operation modes. The cells were anode-supported, the NiO-YSZ microtubular supports being made by Powder Extrusion Moulding (PEM). The cells showed power densities of 695 $mW \cdot cm^{-2}$ at 800 °C and 0.7 V in SOFC mode, and of 845 $mA \cdot cm^{-2}$ at 800 °C and 1.3 V in SOEC mode. AC impedance experiments performed under different potential loads demonstrated the reversibility of the cells. These results showed that these cells, prepared with a method suitable for using on an industrial scale, are highly reproducible and reliable, as well as very competitive as reversible SOFC-SOEC devices operating at intermediate temperatures.

Keywords: Electrochemical properties, extrusion, microtubular, SOFC, SOEC

1. Introduction

Fuel cells are devices that convert the chemical energy stored in a fuel into electricity through a chemical reaction of a fuel (hydrogen) with an oxidizing agent (air). They show high conversion efficiency and low emission of pollutants. The Solid Oxide Fuel Cells (SOFC), among the different types of cells, require high operating temperature (500-1000 ºC), showing in return high fuel flexibility [1].

SOFCs can operate reversibly, producing hydrogen from steam in the Solid Oxide Electrolysis Cell mode (SOEC). The resulting hydrogen can be stored and subsequently used to generate electricity and heat in SOFC mode [2,3,4]. The use of reversible systems is of great interest in terms of reducing the costs. One single device can be used in electrolyser mode to produce hydrogen from intermittent renewable sources (e.g., wind or solar energy), and then to generate electricity, in fuel cell mode, when the demand increases. Moreover, SOEC can exploit waste heat from high temperature industrial processes (e.g. nuclear) to increase their nominal efficiency [5,6].

The ideal electrolyte material for both SOFC and SOEC has to be stable in a wide oxygen partial pressure (pO_2) range, with good oxygen ion conduction properties, and presenting no reactivity with other cell components at the preparation and operation temperatures. Conventional yttria stabilized zirconia (YSZ) fulfils most of these requirements. This compound typically presents an acceptable value of ionic conductivity in the range of the working temperature of SOFCs and SOECs, good sinterability and good thermal and mechanical properties. This is the main reason why YSZ still remains a very competitive electrolyte material in these devices [7,8,9].

The most commonly used fuel electrode material is the traditional Ni-YSZ cermet [10]. In turn, lanthanum strontium manganite (LSM) and YSZ-LSM composites are the most frequently used oxygen electrode materials for SOFC/SOEC applications at

high temperatures (>800ºC). Current research aims to reduce the working temperature of electrochemical cells, especially in SOFC mode, between 500 and 750 °C, which prevents many of the inconveniences associated with operation at high temperatures. Inexpensive conventional metals for the stack components can be used, minimizing thermal degradation and the deleterious effects of chemical reactions between cell components [11,12], and also improving the durability. Alternative oxygen electrode materials for applications below 800ºC have been studied in detail, including lanthanum strontium ferrite (LSF) [13, 14, 15], lanthanum strontium cobaltite (LSCo) [14], lanthanum strontium copper ferrite (LSCuF) [13], lanthanum strontium cobalt ferrite (LSCF) [13, 16] or nickelate based materials [17,18]. However, SOEC technology still presents some critical problems that hinder its application in the energy platform [5]. One of the major problems of SOEC devices is the delamination of the oxygen electrode. This is especially severe in the case of lanthanum strontium manganite LSM-YSZ composite electrodes, where delamination is caused by the accumulation of oxygen ions at the electrolyte-electrode interface under high current densities [19,20]. As a consequence, more efficient oxygen electrodes are required to achieve adequate oxygen evolution without overpressure at the electrolyte/electrode interface. In the present paper we propose the $La_{0.6}Sr_{0.4}Co_{0.2}Fe_{0.8}O_{3-\delta}$ (LSCF), that is a mixed electronic ionic conductor (MIEC), as the oxygen electrode. LSCF has been previously proposed by many different authors as the oxygen electrode for SOEC applications, but in planar configuration [2,13,16,21,22,23,24,25]. One of the most remarkable results is that of Schefold *et al.* [26], where they operate an electrolyte supported planar solid oxide cell in the steam-electrolysis mode for more than 23,000 hours, with a current density of j=−0.9 A·cm^{-2}. The cell consisted of a scandia/ceria doped zirconia electrolyte (6Sc1CeSZ), GDC diffusion-barrier/adhesion layers, LSCF as the oxygen electrode, and

a Ni/GDC as the fuel electrode, obtaining a very low degradation rate (0.57%/1000 h). After dismantling, the cell showed no mechanical damage at the electrolyte and H_2/H_2O electrode. Furthermore, it is well known that the addition of an ionic conductor phase, such as YSZ or GDC, enhances the electrochemical performance of the oxygen electrode. Although LSCF is a MIEC presenting substantial ionic conductivity and the electrochemical reaction occurs at both the electrode surface and the bulk, the addition of an ionic conducting phase, such as GDC into LSCF, enhances the ionic conductivity and reduces the polarization resistance of pure LSCF cathodes, especially at low temperatures [27,28].

However, the main drawback of the LSCF-YSZ electrode-electrolyte pair is the reactivity of YSZ with the oxygen electrode material, for example developing insulating phases such as $La_2Zr_2O_7$ and $SrZrO_3$ [29]. Barrier layers between the electrolyte and the oxygen electrode, such as GDC, are used to avoid this reactivity [30,31,32,33].

Within the different configurations of SOFC (planar, tubular and micro-tubular), the microtubular geometry is characterized by a low thermal mass that allows devices with a rapid start-up and shutdown, high volumetric power densities, better mechanical strength and thermal shock resistance [34,35,36]. Cell composition and microstructure play a primary role in SOFC electrochemical performance, and the processing path usually determines those parameters. In this sense, fabrication methods have to be reproducible and scalable, powder extrusion moulding (PEM) being one of the most promising methods for massive microtubular substrate production because of its low-cost, well-established methodology and good standardization of the final product [37]. As a consequence, microtubular SOFCs (mT-SOFC) with supports fabricated by PEM, are excellent candidates for portable applications and they can also be used for high temperature steam electrolysis in the sector of low power devices [38,39]. In addition

mT-SOFC's are excellent for the laboratory testing of SOFC devices because they are cheap and simple to handle. Most of the technological problems can be easily and accurately studied in mT-SOFC's.

Although the use of reversible SOFC/SOEC systems presents a wide range of potential applications, they are still under development because high temperature stable electrodes are required in both operation modes [40,41,42]. This work presents a detailed SOFC–SOEC analysis of anode-supported mT-SOFC cells, with porous Ni-YSZ fuel electrode supports fabricated by PEM, a thin dense YSZ electrolyte layer, a porous thin GDC barrier layer and a porous LSCF-GDC/LSCF double oxygen electrode. It aims to provide detailed information about the behaviour of LSCF oxygen electrodes in microtubular cells operated in reversible SOFC and SOEC mode. Special attention will be paid to the electrolysis operation mode.

2. Material and Methods

2.1. Fabrication of microtubular cells

Anode-supported tubes were prepared by powder extrusion moulding (PEM) following the procedure described by Arias-Serrano *et al.* [43] and Monzón *et al.* [37]. For this purpose, the final composition of the anodic support is 25% nickel and 25% YSZ (TZ-8YS Tosoh, d_{50}=0.9 μm) in volume, after reducing NiO (Hart Materials, Grade F, d_{50}=0.7 μm) to Ni. The anode porosity was adjusted to 50% using corn starch as pore former. The morphology of starch powders used in this work has been recently published [43]. They present irregular prismatic shapes with a relatively narrow particle size distribution, d_{50} = 10 μm, as measured by laser diffraction in Mastersizer 2000 equipment. Subsequently, YSZ electrolyte suspensions were deposited on the mT

supports by dip-coating. These suspensions were prepared using TZ-8YS (Tosoh, d_{50}=0.9 µm) powders in an isopropanol–ethanol azeotropic mixture, with PVB (polyvinyl butyral) as binder and Beycostat (phosphate ester) as dispersant agent. The rheology of suspensions was controlled to achieve optimum processing conditions. In particular, the composition of the colloids was adjusted to get the adequate viscosity for proper filling of mould without entrapping air bubbles. The half-cells were dried at room temperature and co-sintered at 1500 ºC for 2 hours in air. GDC, LSCF-GDC and LSCF suspensions were prepared using GDC ($Ce_{0.9}Gd_{0.1}O_{2-d}$, Fuel Cell Materials, d_{50}=0.1-0.4 µm) and LSCF ($La_{0.6}Sr_{0.4}Co_{0.2}Fe_{0.8}O_{3-\delta}$, Fuel Cells Materials, d_{50}=0.7-1.1 µm) powders with an appropriate amount of solvent (ethanol), binder (PVB) and dispersant (Beycostat), following the same preparation described elsewhere [33]. GDC barrier layer suspensions were also deposited by dip-coating, dried at RT and sintered at 1400 °C for 2 hours in air. Then, LSCF-GDC and LSCF oxygen electrode suspensions were also deposited by dip-coating, dried at RT and sintered at 1150 ºC for 2 hours in air, each independently. The oxygen electrode active area was limited to 1 cm^2.

2.2. Microstructural and electrochemical characterization

Microstructural characterization was performed in polished transverse cross-sections using a field-emission scanning electron microscopy (model Merlin from Carl Zeiss, Germany) equipped with an energy dispersive analytical system (EDS) for characteristic X-ray analysis (INCA450, Oxford Instruments, UK). Open and connected porosity of the anode supports was measured by means of an Hg porosimeter (Poremaster, Quantachrome; maximum pressure 30,000 psi). Total porosity of the anode supports was determined by gravimetric density measurement. Electrochemical characterization was carried out in both SOFC and SOEC modes using the experimental

setup described elsewhere [4, 44,45]. The cells were heated up to 800 ºC under nitrogen atmosphere and then switched to humidified hydrogen for a period of 24 hours, in order to assure full accommodation of the nickel particles after NiO reduction [46,47]. The fuel composition used was of 3% H_2O – 97% H_2 for operation in the fuel cell mode, and 50% H_2O – 50% H_2 in reversible SOFC-SOEC experiments. Electrical contacts were made using silver and gold wires. For the inner contact (fuel electrode), Ag wires were coiled and mechanically attached into featured holes (visible in figure 1 b) on both ends of the Ni-YSZ microtubes. For the outer contact (oxygen electrode), Au wire was coiled around the surface of the electrode (~1 cm^2), adding Au paste to improve electrical contact and current collection, as shown in figure 1 (b). The cells were characterized in the 600-800 °C temperature range using a potentiostat/galvanostat (VSP), fitted with a frequency response analyser (Princeton Applied Research, Oak Ridge, US). Potentiodynamic experiments were performed from the Open Circuit voltage (OCV) down to 0.5 V at a rate of 0.25 $mA \cdot s^{-1}$. Chronoamperometric studies were also performed fixing the voltage at 0.7 V. Electrochemical impedance spectroscopy (EIS) was performed at OCV under ±200 mA current load, using a sinusoidal signal with 50 mV of amplitude, in the frequency range of 500 kHz to 0.1 Hz. All measurements were normalized by 1 cm^2 of the oxygen electrode outer surface area.

3. Results and discussion

3.1. Cell Microstructure

The micro-tubular cells were 50 mm in length and with an external diameter of 3.4 mm, as can be seen in figures 1 (a) and (b). The thickness of the different ceramic layers were: fuel electrode about 400 μm; electrolyte ~20 μm; GDC barrier layer ~2–4

μm; LSCF-GDC oxygen electrode about 50 μm and LSCF current collector about 30 μm.

Typical microstructure of the Ni-YSZ|YSZ|GDC|LSCF-GDC|LSCF cell is shown in Figure 1 (c, d and e). The microstructure of the Ni-YSZ supports (figure 1 c) has been previously reported by Arias-Serrano *et al.* [43]. This electrode presented a total porosity of about 43%, as determined by gravimetric measurements, where 35% corresponds to open porosity, as obtained from Hg porosimetry experiments. These measurements were performed after sintering and reduction of NiO to Ni. The pore size distribution is bimodal, with spherical pores of about 4-6 μm in agreement with the size of the pore former (corn-starch), and pores in the range <1 μm due to reduction of NiO grains. The electrolyte is nearly fully dense, only presenting a little amount of small closed pores. The thin GDC barrier layer is porous and continuous throughout the electrolyte–oxygen electrode interface, as can be distinguished in figure 1(e) by a darker contrast than the oxygen electrode. The double layer oxygen electrode/current collector (LSCF-GDC/LSCF) is also porous and continuous, as observed in figure 1(d). Good adhesion between layers is observed at all the different interfaces. It is interesting to point out that the composition and microstructure of these cells are similar to those reported in reference [33], where the support was fabricated by cold isostatic pressing (CIP-SOFC). However, as will be shown later on, the performance of the new cells improves that of the CIP-SOFC.

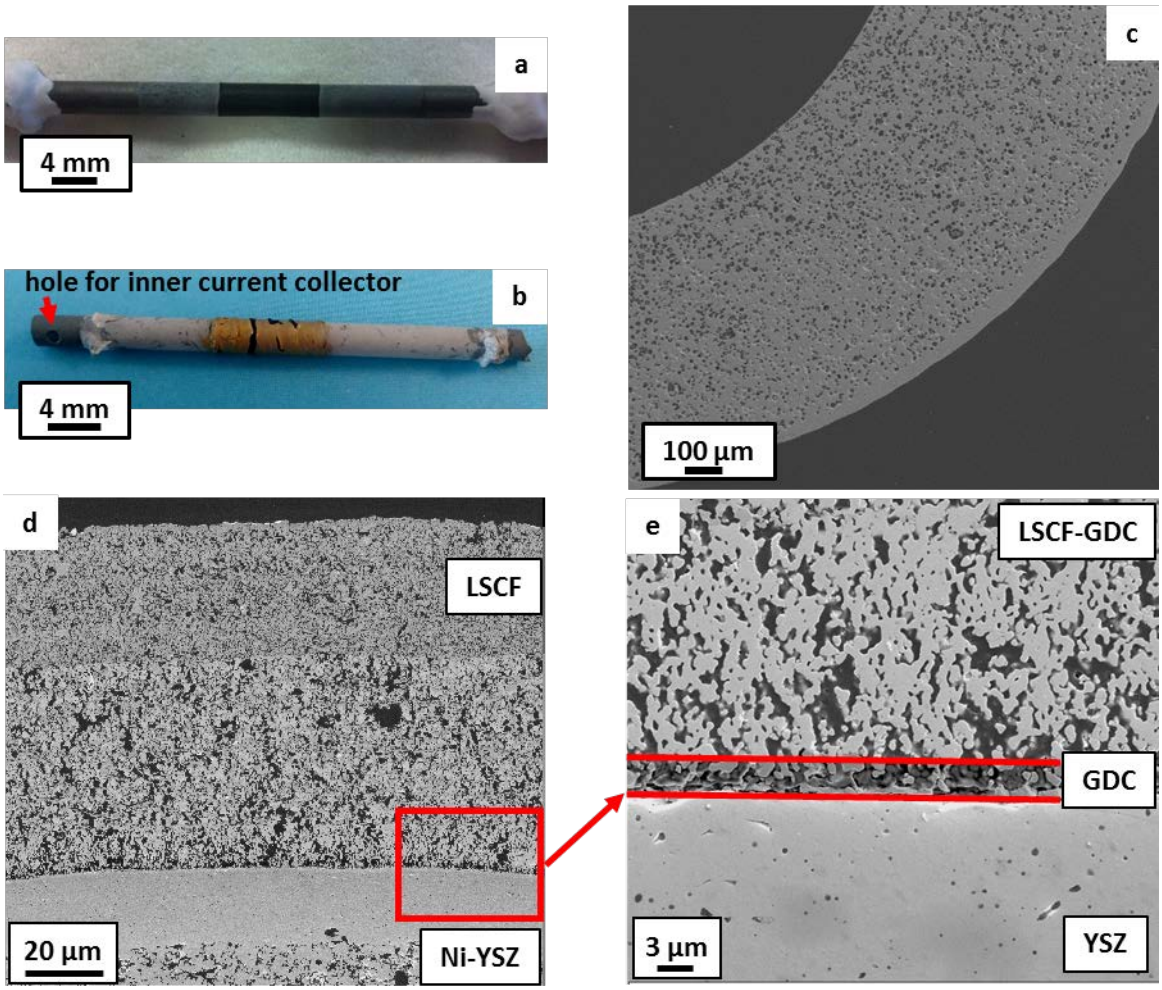

Figure 1. Images corresponding to a mT-SOFC cell with the Ni/YSZ support fabricated by PEM. a) The cell without current collectors mounted in the fuel pipes. b) An operated cell showing details of electrode connectors. c) SEM image of polished transverse cross-section, showing the typical microstructure of the YSZ coated cylindrical YSZ/NiO support. d) SEM image of polished transverse cross-section showing the typical microstructure of Ni-YSZ|YSZ|GDC|LSCF-GDC|LSCF microtubular cell. e) SEM image showing the GDC barrier layer.

r

3.2. Electrochemical characterization

3.2.1. SOFC analysis

In order to study the electrochemical response of the cells in SOFC mode, potentiodynamic studies were performed using pure humidified hydrogen (3% H_2O – 97% H_2) as fuel (0.08 $l \cdot min^{-1}$) and static air as oxidant. The experiments were

performed at temperatures from 600 ºC to 800 ºC and the *j*-V (current density vs. voltage) and *j*-P (current density vs. power density) results are given in Figure 2. Three identical cells using the same composition were electrochemically tested and their performance was very reproducible, as can be observed on the *j*-V curve at 800 ºC (figure 2).

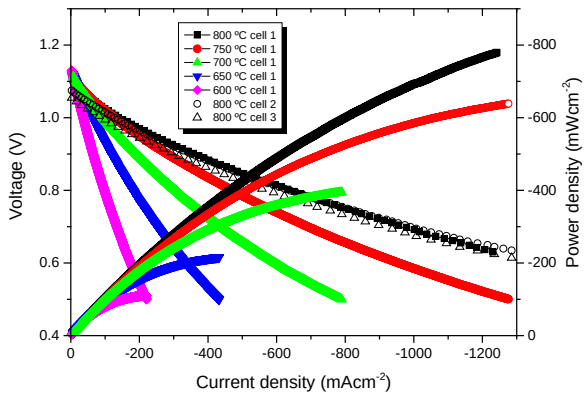

Figure 2. *j*-V and *j*-P curves measured at temperatures from 600 ºC to 800 ºC for three cells of the same composition.

The OCV (Open Circuit Voltage) values are given in Table 1. All OCV values correspond to those predicted by the Nernst equation, assuring both adequate cell sealing and tightness of the YSZ electrolyte. A summary of the electrochemical properties of these cells, whose electrode supports were fabricated by PEM (named "PEM-SOFC"), is shown in Table 1 and also compared with a standard cell of identical composition where the support was fabricated by CIP (called "CIP-SOFC") [33]. As observed in the table, the performance of the PEM cells is better than the standard CIP cells for all the range of studied temperatures. This stems from better homogeneity and surface quality of the fuel electrode support fabricated by PEM process, which possibly results in better integration of the PEM support with the YSZ electrolyte. The reported performances are also superior to similar mT-SOFC's where the Ni-YSZ anode support was also fabricated by PEM, but with LSM-YSZ (-0.64 A·cm^{-2} at 0.7 V) [37] or with

nickelate-based oxygen electrodes (-0.9 $A \cdot cm^{-2}$ at 0.7 V) [39]. In conclusion, the performance of these PEM-SOFC cells is superior to previous CIP-SOFC's and very competitive when compared to similar LSCF microtubular cells reported in the literature. For instance, the best values reported for the current density at 0.7 V and 700 ºC are j=-330 $mA \cdot cm^{-2}$ [48] and j=-990 $mA \cdot cm^{-2}$ [49], other cells presenting similar characteristic values [50, 51, 52].

Table 1. Experimental and calculated OCV values, Current density at 0.7 V, electrical power at 0.5V and Area Specific Resistance values obtained from the *j-V* curves for the cells.

Cell	Temperature	OCV (V) Experimental	OCV (V) Calculated	j ($mAcm^{-2}$) at 0.7 V	P_{max} ($mWcm^{-2}$) at 0.5 V	ASR_{cell} (Ωcm^2) at 0.5 V
CIP-SOFC [33]	650 °C	1.13	1.13	-185	160	1.97
	700 °C	1.13	1.12	-320	280	1.10
	750 °C	1.12	1.11	-525	460	0.67
	800 °C	1.11	1.10	-795	695	0.44
PEM-SOFC	600 °C	1.14	1.14	-135	110	2.91
	650 °C	1.13	1.13	-250	215	1.46
	700 °C	1.13	1.12	-440	395	0.80
	750 °C	1.12	1.11	-690	640	0.48
	800 °C	1.10	1.10	-970	1050*	0.28*

* Data extrapolated at 0.5 V from experimental data.

3.2.2. Reversible operation analysis

Reversible operation experiments in both SOFC and SOEC modes were performed for the PEM-SOFC cell using 50% H_2/50% H_2O as fuel and synthetic air ($p(O_2)$ = 0.21 atm) as oxidant. As shown in Figure 3, the PEM-SOFC cell behaviour is fully reversible in the range of temperatures studied (600–800 ºC). Concentration

polarization is observed in both operation modes at about ±1 A·cm^{-2}. For example, in SOEC mode (at 800 ºC and 1.3 V), current densities of 845 mA·cm^{-2} and ASR values of 0.40 Ω·cm^2 were measured. As far as we know, this current density value is the highest reported for a microtubular electrolyser, as seen in Table 2. For instance Li *et al*. obtained a current density of about 625 mA·cm^{-2} at 1.3 V and 800 ºC using H_2/H_2O (40/60) as fuel in Ni-YSZ/YSZ/LSM-YSZ microtubular cells [53], whereas Hanifi *et al.* reported 780 mA·cm^{-2} in the same operation conditions using H_2/H_2O (50/50) as fuel in the same type of cells but with nanoparticles infiltrated in both electrodes [54]. Other values reported are even lower [55, 56, 57, 58, 59, 60, 61, 62], as summarized in Table 2. In addition, the performance of the cells reported in this paper is not far from that of more developed planar high temperature electrolysers with the same components. For example, Schefold *et al.* reported current densities of 1 A·cm^{-2} at ~1.1 V at about 780 ºC using cells fabricated at Forschungszentrum Jülich [63]. Similar values were reported for cells fabricated at DTU (1.2 A·cm^{-2} at 1.3V at 800 ºC) [6] or POSTECH (1.4 A·cm^{-2} at 1.3V at 800 ºC) [64].

Table 2. Comparison of electrochemical performance of other mT-SOFC's in electrolysis mode

Cell composition	Fuel composition	Temperature (ºC)	j (mAcm^{-2}) at 1.3 V	Reference
Ni-YSZ|YSZ|GDC|GDC-LSCF|LSCF	H_2/H_2O (50/50)	800	845	This work
Ni-YSZ|YSZ|LSM-YSZ	H_2/H_2O (50/50)	800 ºC	100	[55]
Ni-YSZ|YSZ|GDC-PNO|PNO	H_2/H_2O (50/50)	800 ºC	780	[11]
Ni-YSZ|YSZ|LSM-YSZ	H_2/H_2O (50/50)	820 ºC	550	[12]
Ni-YSZ|YSZ|LSM	H_2/H_2O (50/50)	820 ºC	320	[56]
Ni-ScSZ|ScSZ|GDC|LSCF-GDC	H_2/H_2O (82/18)	800 ºC	70	[57]
Ni-ScSZ|ScSZ|GDC|LSCF-GDC	H_2/H_2O (40/60)	650 ºC	550	[58]
Ni-YSZ|YSZ|LSM-YSZ	H_2/H_2O (40/60)	850 ºC	600	[59]
Ni-YSZ|YSZ|LSM-YSZ	H_2/H_2O (40/60)	800 ºC	625	[53]
Ni-YSZ|YSZ|LSM-GDC-YSZ	H_2/H_2O (70/30)	900 ºC	670	[60]
Ni-YSZ|YSZ|LSM-YSZ|LSM	H_2/H_2O (25/75)	822 ºC	520	[61]
Ni-YSZ|YSZ|LSM-YSZ	H_2/H_2O (50/50)	800 ºC	780	[54]
Ni-YSZ|YSZ|NNO-YSZ	H_2/H_2O (50/50)	800 ºC	585	[62]

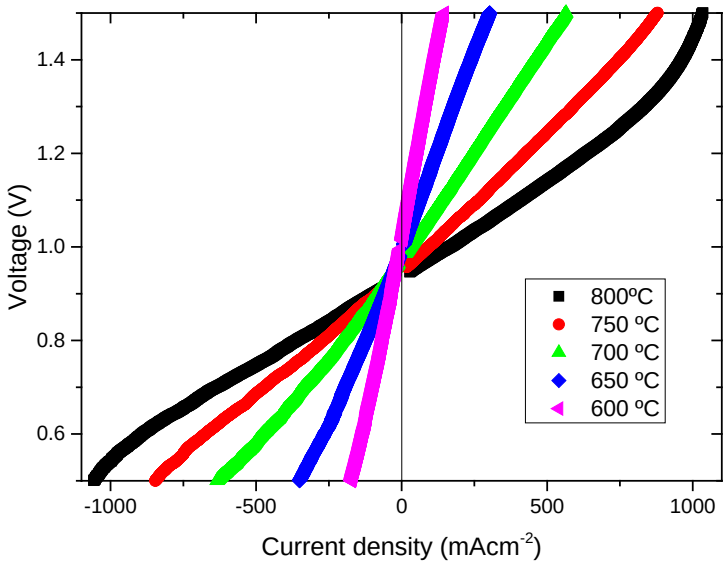

Figure 3. *j–V* curves (SOEC and SOFC modes) performed for the PEM-SOFC cell at different temperatures

EIS analysis under OCV conditions was performed before and after the *j*-V measurements in order to confirm that there is no degradation during current load in both operation modes. In addition, EIS under both anodic (SOFC: +200 mA) and cathodic (SOEC: -200 mA) polarization was performed. The results at 800 ºC are shown in figure 4. All data was fitted using the equivalent circuit L-R_o-$(RQ)_1$-$(RQ)_2$-$(RQ)_3$, where L is the inductance, R is the resistance and Q is the constant phase element. The fitting parameters are summarized in table 3. Based on previous studies of similar cells using PNO electrodes [31], the different components were assigned as follows: R_1 was attributed to charge transfer mechanism at the oxygen electrode, R_2 and R_3 were attributed to gas mass transfer at the oxygen electrode and fuel electrode, respectively. Charge transfer at the fuel electrode is either negligible or could be overlapped with R_1, especially for operation at the lower temperatures. This ascription is corroborated as,

according to values in table 4, the most significant changes were observed in the component assigned to charge transfer at the oxygen electrode (R_1), which is reduced under SOFC mode and increased under SOEC mode. As expected, slightly lower ASR values were found in SOFC mode than in SOEC mode for this cell. This trend is also compatible with the slopes of the *j*-V curves (figure 3) and also with the typical behaviour of electrolysers when using LSM-YSZ oxygen electrodes. Virkar's prediction of higher oxygen overpotentials being built at the oxygen electrode/electrolyte during electrolysis operation explains this tendency [65]. However, this is not the case when cells are fabricated using oxygen excess phases, such as $La_{2-x}Sr_xCo_{0.5}Ni_{0.5}O_{4\pm\delta}$, in the oxygen electrodes [39, 66]. This hyperstoichiometry seems to be favourable in electrolysis mode operation.

Table 3. Impedance parameters fitted from the EIS experiments.

	Resistance				
Temperature (ºC)	**R_0 (Ωcm^2)**	**R_1 (Ωcm^2)** 0.5-20 kHz ~10^{-4} Fcm^{-2}	**R_2 (Ωcm^2)** 50-200 Hz ~10^{-2} Fcm^{-2}	**R_3 (Ωcm^2)** 5-10 Hz 0.1-0.4 Fcm^{-2}	**ASR (Ωcm^2)**
800 OCV	0.23 (1)	0.04 (1)	0.04 (1)	0.07 (1)	0.38 (4)
800 SOFC	0.23 (1)	0.03 (1)	0.04 (1)	0.07 (1)	0.37 (4)
800 SOEC	0.23 (2)	0.05 (1)	0.04 (1)	0.07 (1)	0.39 (5)
750 OCV	0.36 (1)	0.07 (1)	0.06 (1)	0.08 (1)	0.58 (4)
750 SOFC	0.36 (1)	0.04 (1)	0.06 (1)	0.07 (1)	0.53 (4)
750 SOEC	0.36 (1)	0.09 (1)	0.06 (1)	0.08 (1)	0.59 (4)
700 OCV	0.58 (2)	0.14 (1)	0.11 (1)	0.07 (1)	0.91 (5)

700 SOFC	0.61 (3)	0.07 (1)	0.14 (1)	0.06 (1)	0.88 (6)
700 SOEC	0.59 (2)	0.19 (1)	0.08 (1)	0.08 (1)	0.95 (5)
650 OCV	1.07 (2)	0.23 (1)	0.24 (2)	0.05 (1)	1.59 (6)
650 SOFC	1.09 (2)	0.14 (1)	0.15 (1)	0.06 (1)	1.45 (5)
650 SOEC	1.04 (4)	0.36 (3)	0.17 (1)	0.07 (1)	1.64 (9)
600 OCV	2.13 (1)	0.78 (2)	0.43 (2)	0.09 (1)	3.43 (6)
600 SOFC	2.05 (2)	0.21 (2)	0.24 (1)	0.09 (1)	2.59 (6)
600 SOEC	2.02 (3)	0.84 (3)	0.05 (1)	0.10 (1)	3.02 (8)

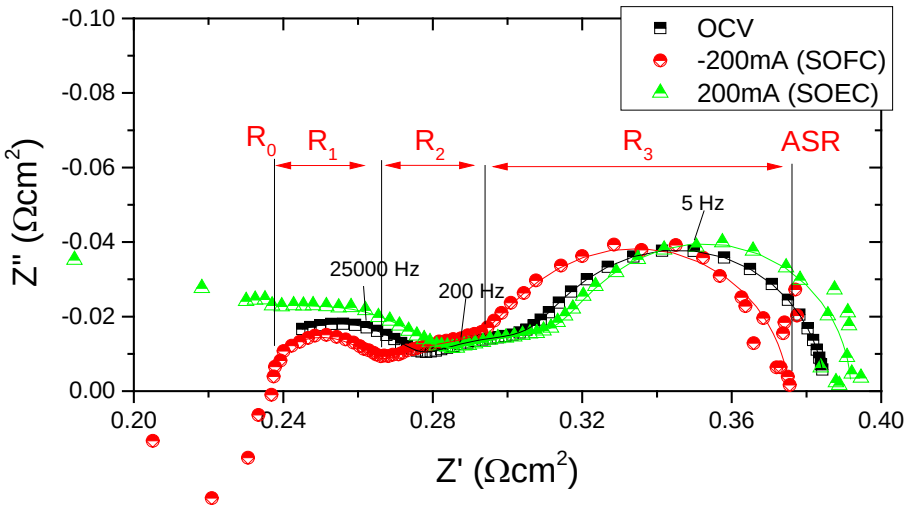

Figure 4. EIS analysis performed at OCV and under current load for the PEM-SOFC cell at 800 ºC

3.2.3. Short-term durability

A chronoamperometric study in SOFC and SOEC modes was performed to obtain information about the short-term durability of the cells. The first study was performed in SOFC operation mode, at 800 ºC and at a fixed voltage of 0.8 V, using pure humidified hydrogen (3% H_2O – 97% H_2) as fuel and static air as oxidant. The results

are given in Figure 5 (left) for a period above 260 hours. During this time there is no apparent degradation of the cell, as the current density remains constant. Subsequent to this experiment, the cell was switched to SOEC mode by fixing the voltage at 1.2 V. Unfortunately a current lead broke and the experiment stopped after 6.5 hours operation in SOEC mode as shown in figure 5 (right). During this period, the performance of the cell increased slightly, as was also confirmed by the *j*-V measurement collected after the chronoamperometric study (see inset in figure 5 left). SEM analysis of the cell after operation also confirmed that there is no observable deterioration of the cell. New experiments are programmed for longer time duration experiments in SOEC mode.

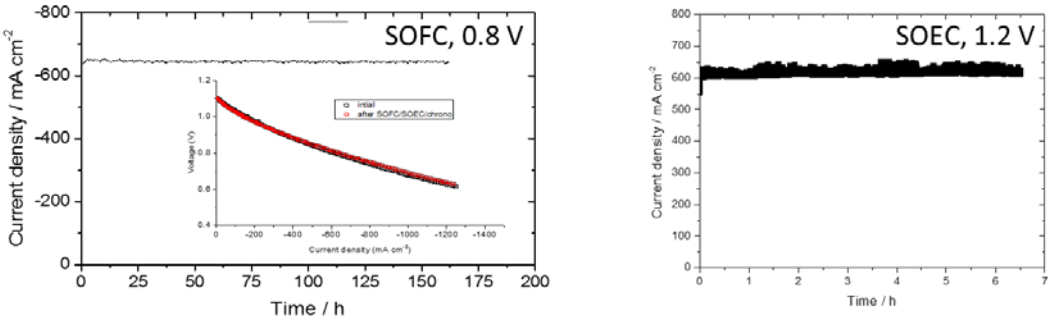

Figure 5. Chronoamperometric study for the PEM cell at 800 ºC and 0.8V for 260 hours (SOFC mode, left); and at 1.2V for 6.5 hours (SOEC mode, right). The inset of figure 5 (left) shows the *j–V* curves (SOFC mode) performed before and after the chronoamperometric study

4. Conclusions

mT-SOFC anode supported cells have been fabricated using YSZ:Ni supports made by the powder extrusion method (PEM) and the dip coating technique to deposit the YSZ electrolyte, GDC protection barrier and GDC-LSCF electrodes. The fabrication method leads to cells with a high homogeneity, excellent surface finishing and very

reproducible behaviour. The cell performance is superior to previous ones where the support was fabricated by CIP. Cells were tested in both SOFC and SOEC modes showing a reversible behaviour pattern and good performance, in both operation modes at temperatures between 600 and 800ºC. As far as we know, this is the highest current density value (845 $mA \cdot cm^{-2}$ at 800 ºC and 1.3 V) reported for a microtubular electrolyser. Durability experiments show no deterioration of cells for a period of 260 hours under SOFC mode and 6.5 hours under SOEC mode.

Acknowledgements

The authors would like to acknowledge the grant MAT2015-68078-R financed by the Spanish Government (Ministerio de Economía y Competitividad) and Feder program of the European Community for funding the project. The use of Servicio General de Apoyo a la Investigación (SAI, University of Zaragoza) is also acknowledged.

References

[1] S.C. Singhal, K. Kendall, High temperature solid oxide fuel cells: fundamental, design and applications. Oxford: Elsevier; 2003.
[2] M.A. Laguna-Bercero, J.A. Kilner, S.J. Skinner, Solid State Ion., 192 (2011), pp. 501–504.
[3] A. Hauch, S.D. Ebbesen, S.H. Jensen, M. Mogensen, J. Mater. Chem., 18 (2008), pp. 2331-2340.
[4] M.A. Laguna-Bercero, R. Campana, A. Larrea, J.A. Kilner, V.M. Orera, Fuel Cells, 11 (2011), pp. 102-107.
[5] M.A. Laguna-Bercero J. Power Sourc., 203 (2012), pp. 4–16.
[6] S.D. Ebbesen, S.H. Jensen, A. Hauch, M. Mogensen, Chem. Rev., 114 (2014), pp. 10697-10734.
[7] N.N. Osada, H. Uchida, M. Watanabe, J. Electrochem. Soc., 153 (2006), pp. A816-A820.
[8] M.A. Laguna-Bercero, S.J. Skinner, J.A. Kilner, J. Power Sourc., 192 (2009), pp. 126-131.
[9] J.E. O'Brien, C.M. Stoots, J.S. Herring, J. Hartvigsen, J. Fuel Cell Sci. Technol., 3 (2006), pp. 213-219.
[10] B.S. Prakash, S.S. Kumar, S.T.Aruna, Renew. Sustain. Energy Rev., 36 (2014), pp. 149–179.
[11] B.C.H. Steele, A. Heinzel, Nature, 414 (2001), pp. 345–352.
[12] V. Lawlor, S. Griesses, G. Buchinger, A.G. Olabi, S.Cordiner, D. Meissner, J. Power Sourc., 193 (2009), pp. 387–399.
[13] O.A. Marina, L.R. Pederson, M.C. Williams, G.W. Coffey, K.D. Meinhardt, C.D. Nguyen, E.C. Thomsen, J. Electrochem. Soc., 154 (2007), pp. B452-B459.

[14] W. Wang, Y. Huang, S. Jung, J.M. Vohs, R.J. Gorte, J. Electrochem. Soc., 153 (2006), pp. A2066-A2070.
[15] J. Kong, Y. Zhang, C. Deng, J. Xu, J. Power Sourc., 186 (2009), pp. 485-489.
[16] G. Schiller, A. Ansar, M. Lang, O. Patz, J. Appl. Electrochem., 39 (2009), pp. 293-301.
[17] M.A. Laguna-Bercero, A.R. Hanifi, H. Monzón, J. Cunningham, T.H. Etsell, P. Sarkar, J. Mater. Chem. A, 2(2014), pp. 9764-9770.
[18] T. Ogier, F. Mauvy, J.-M. Bassat, J. Laurencin, J. Mougin, J.-C. Grenier, Int. J. Hydrogen Energy, 40 (2015), pp. 15885-15892.
[19] Chen, K., Jiang, S.P. Int. J. Hydrogen Energy, 36 (2011), pp. 10541-10549.
[20] MA Laguna-Bercero, VM Orera, Int. J. Hydrogen Energy, 36 (2011), pp. 13051-13058
[21] MA Laguna-Bercero, JA Kilner, SJ Skinner, Chem. Mater. 22 (2010), pp. 1134-1141.
[22] P. Hjalmarsson, X. Sun, Y.-L. Liu, M. Chen, J. Power Sourc. 223 (2013) pp. 349-357.
[23] F. Tietz, D. Sebold, A. Brisse, J. Schefold, J. Power Sourc. 223 (2013) pp. 129-135
[24] H.-J. Choi, Y.-H. Na, M. Kwak, T.W. Kim, D.-W. Seo, S.-K. Woo, S.-D. Kim, Ceram. Int. 43 (2017) pp. 13653-13660
[25] J. Laurencin, M. Hubert, D.F. Sanchez, S. Pylypko, M. Morales, A. Morata, B. Morel, D. Montinaro, F. Lefebvre-Joud, E. Siebert, Electrochim. Acta 241 (2017) pp. 459-476.
[26] J. Schefold, A. Brisse, H. Poepke, Int. J. Hydrogen Energy 42 (2017) pp. 13415-13426.
[27] V. Dusastre, J.A. Kilner, Solid State Ion., 126 (1999), 163–74.
[28] E.P. Murray, M.J. Sever, S.A. Barnett, Solid State Ion., 148 (2002), 27–34.
[29] H.Y. Lee, W.S. Cho, S.M. Oh, Bull. Korean Chem. Soc., 19 (1998), pp. 661–666.
[30] T.L. Nguyen, K. Kobayashi, T, Honda, Y. Iimura, K. Kato, A. Neghisi, K. Nozaki, F. Tappero, K. Sasaki, H. Shirahama, K. Ota, M. Dokiya, T. Kato, Solid State Ion., 174 (2004), pp. 163–174.
[31] S. Uhlenbruck, N. Jordan, D. Sebold, H.P. Buchkremer, V.A.C. Haanappel, D. Stöver, Thin Solid Films, 515 (2007), pp. 4053–4060.
[32] N. Jordan, W. Assenmacher, S. Uhlenbruck, V.A.C. Haanappel, H.P. Buchkremer, D. Stöver, W. Mader, Solid State Ion., 179 (2008), pp. 919–23.
[33] M.J. Lopez-Robledo, M.A. Laguna-Bercero, J. Silva, V.M. Orera, A. Larrea, Ceram. Int., 41 (2015), pp. 7651–7660.
[34] K. Kendall, Int. J. Appl. Ceram. Technol., 7 (2010), pp. 1-9.
[35] V. Lawlor, J. Power Sourc., 240 (2013), pp. 421-441.
[36] V.M. Orera, M.A. Laguna-Bercero, A. Larrea, Front. Energ. Res., 2 (2014), pp. 1-13.
[37] H. Monzón, M.A. Laguna-Bercero, Int. J. Hydrogen Energy, 39 (2014), pp. 5470–5476.
[38] M.A. Laguna-Bercero, R. Campana, A. Larrea, J.A. Kilner, VM Orera, J. Power Sourc., 196 (2011), pp. 8942-8947
[39] M.A. Laguna-Bercero, H. Monzón, A. Larrea, V.M. Orera, J. Mater. Chem. A, 4 (2016), pp. 1446–1453
[40] S. Y. Gómez, D. Hotza, Renew. Sust. Energy Rev., 61 (2016), pp. 155–174.
[41] K. Chen, S.-S. Liu, N. Ai, M. Koyama, S.P. Jiang, Phys. Chem. Chem. Phys., 17 (2015), pp. 31308-31315
[42] S.P. Jiang, Asia-Pac. J. Chem. Eng., 11 (2016), pp. 386-391.
[43] B.I. Arias-Serrano, M.E. Sotomayor, A. Várez, B. Levenfeld, H. Monzón, M. A. Laguna-Bercero, A. Larrea, RSC Adv., 6 (2016) pp. 19007–19015
[44] H. Monzón, M. A. Laguna-Bercero, Int. J. Hydrogen Energy, 37 (2012), pp. 7262-7270.
[45] M. A. Laguna-Bercero, A. Férriz, A. Larrea, L. Correas, V. M. Orera, Fuel Cells, 13 (2013), pp. 1116-1122.
[46] H. Monzón, M. A. Laguna-Bercero, Electrochim. Acta, 221 (2016), pp. 41-47.
[47] H. Monzón, M. A. Laguna-Bercero, Electrochim. Acta, 222 (2016), pp. 1622-1627.
[48] S.Y. Park, J. H. Ahn. C.-W. Jeong, C. W. Na. R.-H. Song. J.-H.Lee, Int. J. Hydrogen Energy, 39 (2014), pp. 12894–12903.
[49] M. Torrell, A. Morata, P. Kayser, M. Kendall, K. Kendall, A. Tarancón., J. Power Sourc., 285 (2015), pp. 439–448.
[50] T. Yamaguchi, N. Sammes, ECS Trans., 33 (2011), pp. 143-148.
[51] H. Sumi, T. Yamaguchi, K. Hamamoto, T. Suzuki, Y. Fujishiro, T. Matsui, K. Eguchi, Electrochim. Acta, 67 (2012), pp. 159–165.
[52] H. Sumi, D. Kennouche, K. Yakal-Kremski, T. Suzuki, S. A. Barnett, D. J. Miller, T. Yamaguchi, K. Hamamoto, Y. Fujishiro, Solid State Ion., 285 (2016), pp. 227–233.
[53] Y. Li, L. Chen, L. Zhang, C. Xia, Int. J. Hydrogen Energy, 41 (2016), pp. 5209–5214.

[54] A.R. Hanifi, M.A. Laguna-Bercero, T.H. Etsell, P. Sarkar, Int. J. Hydrogen Energy, 39 (2014), pp. 8002–8008.
[55] T. Mizusawa, T. Araki, M. Mori, Int. J. Hydrogen Energy, 41 (2016), pp. 13888–13900.
[56] M.A. Laguna-Bercero, R. Campana, A. Larrea, J.A. Kilner, V.M. Orera, J. Electrochem. Soc., 157 (2010), pp. B852-B855.
[57] S. Hashimoto, Y. Liu, M. Mori, Y. Funahashi, Y. Fujishiro, Int. J. Hydrogen Energy, 34 (2009), pp. 1159-1165.
[58] Z. Wang, M. Mori, T. Araki, Int. J. Hydrogen Energy, 35 (2010), pp. 4451 – 4458.
[59] C. Jin, C. Yang, F. Chen, ECS Transactions, 35 (2011), pp. 2987-2995.
[60] C. Yang, C. Jin, F. Chen, Electrochim. Acta, 56 (2010), pp. 80–84.
[61] L. Kleiminger, T. Li, K. Li, G.H.Kelsall, Electrochim. Acta, 179 (2015), pp. 565–577.
[62] A. R. Hanifi, M. A. Laguna-Bercero, N. K. Sandhu, T. H. Etsell, P. Sarkar, Sci. Rep., 6 (2016), pp. 27359.
[63] J. Schefold, A. Brisse, F. Tietz, J.Electrochem. Soc., 159 (2012), pp. A137-A144.
[64] S. J. Kim, S. W. Kim, Y. M. Park, K. J. Kim, G. M. Choi, Solid State Ion., 295 (2016), pp. 25–31.
[65] A.V. Virkar, Int. J. Hydrogen Energy, 35 (2010), pp. 9527–9533.
[66] M.A. Laguna-Bercero, N. Kinadjan, R. Sayers, H. El Shinawi, C. Greaves, S.J. Skinner, Fuel Cells, 11 (2011), pp. 102-107.